Available online at www.sciencedirect.com
SCIENCE DIRECT®
ELSEVIER
Microelectronic Engineering 69 (2003) 228–236
MICROELECTRONIC ENGINEERING
www.elsevier.com/locate/mee

Proton exchanged $LiNbO_3$ and $LiTaO_3$ optical waveguides and integrated optic devices

Yu.N. Korkishko[a,*], V.A. Fedorov[a], S.M. Kostritskii[a], A.N. Alkaev[a], E.I. Maslennikov[a], E.M. Paderin[a], D.V. Apraksin[a], F. Laurell[b]

[a]*Moscow Institute of Electronic Technology (Technical University), 124498 Moscow, Zelenograd, Russia*
[b]*Department of Physics II, Royal Institute of Technology, S-10044 Stockholm, Sweden*

Abstract

We show that proton exchanged $LiNbO_3$ waveguides exhibit very complex structural chemistry. Seven $H_xLi_{1-x}NbO_3$ and six $H_xLi_{1-x}TaO_3$ crystallographic phases have been identified in PE $LiNbO_3$ and $LiTaO_3$ waveguides, respectively. A correlation is done between the electrooptical, nonlinear and photorefractive properties, the processing conditions and the refractive index changes of the waveguides. Some integrated optical devices have been realized.

Keywords: Lithium niobate; Lithium tantalate; Proton exchange; Optical waveguides; Integrated optical devices

1. Introduction

Lithium niobate, $LiNbO_3$, is a material of considerable interest to the optical, laser and communications industry, due to its large values of electro-optic, nonlinear optical, piezoelectric and acousto-optical coefficients. Lithium tantalate, $LiTaO_3$, is also an attractive host material for integrated-optic devices due to its large electro-optic and nonlinear coefficients, comparable with those of lithium niobate, and its high threshold for photorefractive damage, known to be more than an order of magnitude larger than that of $LiNbO_3$ in the visible spectral range [1]. Guided-wave devices implemented in this material have exhibited a much higher power handling capability [1,2] than $LiNbO_3$, making them ideal for a variety of high-throughput applications.

The proton exchange (PE) method [3] has been used for several years to form optical waveguides in these crystals. Exchanging lithium ions with protons in a proton source such as benzoic acid or other organic or inorganic acids, typically at temperatures in the range from 180 to 250 °C, induces an increase of the $LiNbO_3$ and $LiTaO_3$ extraordinary refractive indices of ~0.12 and ~0.03, respectively, while a decrease in the ordinary refractive index of ~0.04 for $LiNbO_3$ and ~0.06 for $LiTaO_3$ at the 633 nm wavelength [4].

Low-loss waveguides with high index increments can be achieved by employing proton exchange [4]. However, some important properties, notably the electro-optic effect and optical nonlinearity, are adversely affected in unannealed (as-exchanged) waveguides and must be restored by post-exchange annealing [4].

Currently, the annealed proton exchange (APE) technique is used for the fabrication of PE $LiNbO_3$ [5] waveguides and almost exclusively for the fabri-

*Corresponding author. Tel.: +7-95-530-1498; fax: +7-95-536-9934.
E-mail address: korkishk@chem.miee.ru (Y.N. Korkishko).

0167-9317/03/$ – see front matter
doi:10.1016/S0167-9317(03)00302-2

cation of $LiTaO_3$ [2] waveguides, because it is simple and can be performed at temperatures below the Curie point.

The aforementioned inconsistency of data is likely to have been caused by the existence of various crystalline phases of the $H_xLi_{1-x}NbO_3$ and $H_xLi_{1-x}TaO_3$ systems [4]. The crystalline structure of PE $LiNbO_3$ waveguides depends on the exchange conditions, and seven crystallographic $H_xLi_{1-x}NbO_3$ phases, the α, κ_1, κ_2, β_1, β_2, β_3, β_4 $H_xLi_{1-x}NbO_3$ phases can be induced in the crystal [6–8]. Our recent studies [9–11] have shown that up to six different phases of $H_xLi_{1-x}TaO_3$, viz. the α, κ, β_1, β_2, β_3 and β_4 phases, can be realized in proton exchanged $LiTaO_3$ layers, depending on exchange and annealing conditions. These $H_xLi_{1-x}NbO_3$ and $H_xLi_{1-x}TaO_3$ phases have been shown to be structured as individual layers in multi-phase waveguides [4].

To adjust waveguide parameters, postexchange annealing (APE waveguides [2,5]) or/and reverse proton exchange [12–17] (RPE or/and REAPE waveguides) could be used. Recently, the soft proton exchange (SPE) process for making waveguides in $LiNbO_3$ [18–21] and $LiTaO_3$ [22] has been proposed by processing in the melt of benzoic acid diluted by lithium benzoate [18–20] or using a melt of stearic acid highly diluted by lithium stearate [21,22]. No phase transitions are formed when α-phase waveguides are obtained by SPE. The basic techniques for fabricating PE waveguides in $LiNbO_3$ or $LiTaO_3$ are illustrated in Fig. 1.

Publications on the subject report rather different results of the electrooptical and nonlinear properties of the PE $LiNbO_3$ and $LiTaO_3$ waveguides, which are related to the difficult task of probing these properties of a PE thin layer at the surface of the $LiNbO_3$ and $LiTaO_3$ crystals, as well as to the existence of various phases in PE $LiNbO_3$ and $LiTaO_3$ waveguides which have not been taken into account in the previous studies. To clarify the situation, here we present investigation of the in-

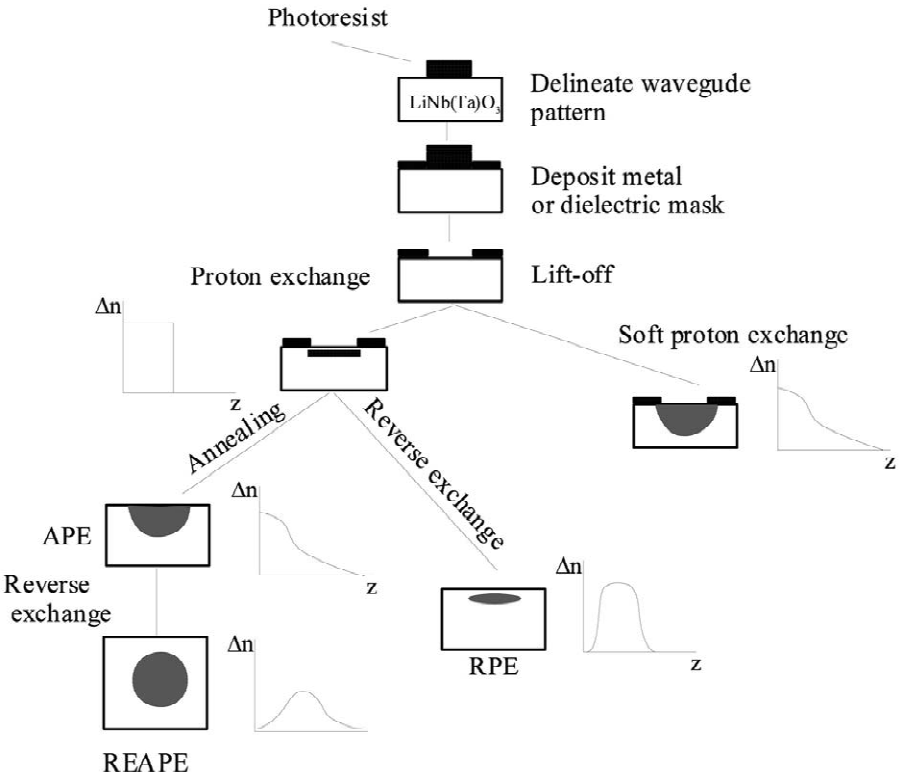

Fig. 1. The family of proton exchange processes in $LiNbO_3$ or $LiTaO_3$.

fluence of the phase state of $H_xLi_{1-x}NbO_3$ and $LiTaO_3$ waveguides, as well as fabrication method (PE, RPE, APE, SPE) on their electrooptical, nonlinear and photorefractive properties.

In Section 5 we will demonstrate some integrated optical devices that can be realized using the PE technique.

2. Preparation of samples and their characterization

In experiments we used optical graded pure X- and Z-cut $LiNbO_3$ and $LiTaO_3$ substrates supplied by Crystal Technology.

Covering a wide range of fabrication parameters to realize the PE waveguides in different $H_xLi_{1-x}NbO_3$ and $H_xLi_{1-x}TaO_3$ phases we used a simple direct exchange, varying the temperature and the acidity of the bath and the duration of the exchange to modify the parameters of the waveguide, as well as a two-step APE process, where the proton exchange is followed by annealing whose duration and temperature further modify the waveguide parameters. The exchanges were realized using as proton sources melts and solutions of different acidity such as pyrophosphoric acid, ammonium dihydrophosphate ($NH_4H_2PO_4$), pure benzoic acid and benzoic acid diluted by lithium benzoate and solutions of $KHSO_4$ in glycerine. APE $LiNbO_3$ waveguides were fabricated by annealing in air at temperatures from 320 to 400 °C.

The reverse proton exchange was performed in eutectic melt $LiNO_3$ (37.5 mol.%)–KNO_3 (44.5 mol.%)–$NaNO_3$ (18.0 mol.%) (melting point of this eutectic mixture is 120 °C) at temperatures from 250 to 330 °C.

Soft proton exchanged waveguides were fabricated in the melt of stearic acid highly diluted by lithium stearate at 370 °C [21].

The obtained planar waveguides were optically characterized using a standard one-prism coupler set-up at 633 nm by measuring excitation angles of dark *m*-lines of modes to calculate the effective indices of modes. The extraordinary refractive index profiles throughout the guide depth were then reconstructed using a generalized Gaussian index model to calculate index profiles in proton-exchanged $LiNbO_3$ waveguides. The profile is given by

$$n(z) = \Delta n_0 \exp\left(-\left(\frac{z}{d}\right)^a\right) \quad (1)$$

where $\Delta n_0 = n_0 - n_s$ is the maximum guide-substrate index change, d is the effective guide depth, and a is a parameter associated with the shape of the profile.

On the same samples, by using a double-crystal X-ray diffractometer DRON-3 (Cu $K\alpha_1$ radiation, Si (311) monochromator) we recorded rocking curves from different crystallographic planes, which we used to calculate the components of the deformation tensor and to reconstruct the surface layer structural properties [23].

From the results of optical and structural characterization we determined the $H_xLi_{1-x}NbO_3$ or $H_xLi_{1-x}TaO_3$ phase composition of the studied sample by using the experimental structural phase diagrams of the PE waveguides on different $LiNbO_3$ and $LiTaO_3$ cuts [6–11] (Figs. 2 and 3). The structural phase diagrams link the measured extraordinary refractive index change Δn_e to the deformation ε''_{33} perpendicular to the crystal surface, which is calculated directly from the rocking curve from the surface plane ((00.12) for Z-cut and (220) for X-cut samples). In these diagrams the phase transitions are characterized by discontinuity of either index variation Δn_e or deformation ε''_{33}. One important point to note from the structural phase diagrams is that the exchanged layers of different $H_xLi_{1-x}NbO_3$ or $H_xLi_{1-x}TaO_3$ phases can generate quite similar index profiles while they differ considerably in structural and other properties. Therefore the knowledge of the crystallographic phases for different waveguides is very important to understand and predict their different, in particular, electrooptical and nonlinear properties.

3. Electrooptical properties of different $H_xLi_{1-x}NbO_3$ and $H_xLi_{1-x}TaO_3$ phases

According to the definition of clamped linear electro-optic coefficient $r_{ij,k}$, a modulating electric field E_k applied to a piezoelectric crystal at frequencies well above sample acoustic resonances, but

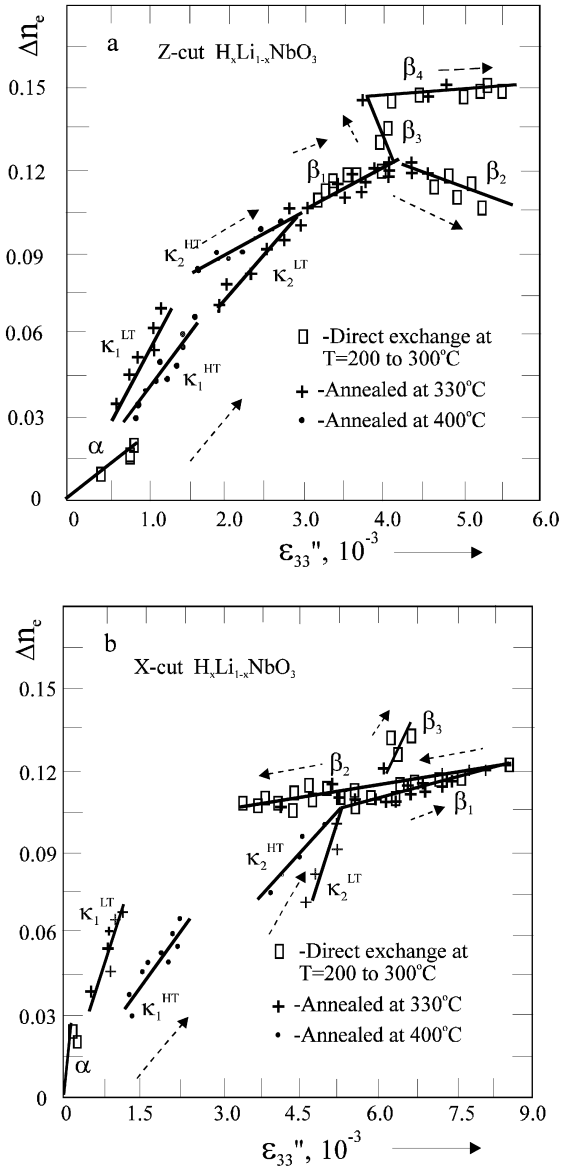

Fig. 2. Structural phase diagrams of $H_xLi_{1-x}NbO_3$ on Z-cut (a) and X-cut (b) substrates. They give the dependence of the extraordinary index variation Δn_e measured at $\lambda = 633$ nm versus the surface value of deformation ε_{33}'' normal to surface plane. The arrows show the directions in which proton concentration increases.

well below lattice optic-mode frequencies, gives a differential optical polarization ($n_i^2 r_{ij,k} n_j^2 E_k E_j$), where n_i and n_j are principal refractive indices at the optical frequencies. The modulating field E_k induces proportional lattice displacements $Q_k^m = \beta_k^m E_k$ in each **m** mode. These displacements in turn cause a perturbation via an electron–phonon interaction in the optical polarization induced by the optical field E_j. An additional perturbation on the polarization is introduced by a direct electron-modulating field interaction in which the lattice remains rigid, as in the case of optical second harmonic generation (SHG). The value of this latter contribution, $\xi_{ijk} E_k E_j$, can be calculated from SHG measurements. The lattice contribution $\alpha_{ij,k}^m \beta_k^m E_k E_j$ can be determined from a combination of Raman scattering and infrared-reflection measurements [24], where $\alpha_{ij,k}^m$ is differential polarizability for the m mode of optical lattice vibration, and coefficients β_k^m can be evaluated from infrared oscillator strength of the m mode.

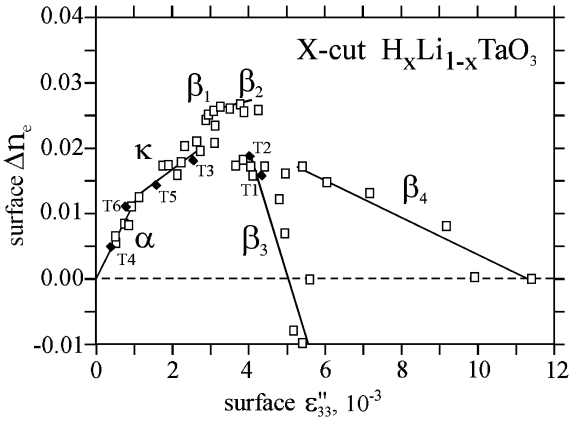

Fig. 3. Structural phase diagram of X-cut $H_xLi_{1-x}TaO_3$ waveguides with positions of the samples studied.

Equating the electro-optic polarization to the sum of lattice and electronic contributions, we have the desired relationship [24,25] between electro-optic, Raman and infrared oscillator parameters

$$n_i^2 r_{ij,k} n_j^2 = \alpha_{ij,k}^m \beta_k^m + \xi_{ijk} \tag{2}$$

summed over m.

In electro-optic measurements, E_k is produced by a low-impedance voltage source connected to electrodes on the crystal. Since the depolarizing field is effectively short-circuited, the local field is that for a transverse optical (TO) mode and the value of $\alpha_{ij,k}^m$ at the TO phonon frequency ω_{TO}^m must be employed in Eq. (2). At frequencies well below ω_{TO}^m, β_k^m is

Table 1
Calculated electrooptical coefficients for different $H_xLi_{1-x}NbO_3$ phases [27]

Phase	α	κ_1^{LT}	κ_2^{LT}	β_1	β_2	β_3	β_4
r_{ij}/r_{ij}^0	0.99	0.91	0.83	0.61	0.58	0.61	0.2

r_{ij}^0, electrooptical coefficients for pure $LiNbO_3$.

given by $(\varepsilon_o \Delta\kappa_k^m v/K_k^m)^{1/2}$, where $\Delta\kappa_k^m$ is the contribution of the m mode to the low-frequency dielectric constant, K_k^m is the spring constant for the m mode, and v is the volume of a unit cell. Thus, using (2) and the well-known relations [25,26] for $\alpha_{ij,k}^m$ and ξ_{ijk}, we have

$$r_{ij,k} = (n_i^2\, n_j^2)^{-1}\{\pm[\,\varepsilon_o \Delta\kappa_k^m\, S_{ij,k}^m/\sigma^m]^{1/2} + 4d_{ijk}\} \quad (3)$$

where $S_{ij,k}^m$ is Raman scattering efficiency for a Stokes line of the m mode, σ^m is a some coefficient, including the Bose population factor and parameters related to experimental conditions, and d_{ijk} is the SHG coefficient. We define the Raman scattering efficiency as the total optical power scattered with polarization i at a Stokes frequency, divided by the total incident power with polarization j.

The IR-reflection data allow to determine the values of $\Delta\kappa_k^m$ for the each polar m mode

$$\Delta\kappa_k^m = (\omega_{TO}^m)^{-2}\,\varepsilon_{k,\infty}\{(\omega_{LO}^m)^2 - (\omega_{TO}^m)^2\}\,\Pi[\{(\omega_{LO}^n)^2 - (\omega_{TO}^m)^2\}/\{(\omega_{TO}^n)^2 - (\omega_{TO}^m)^2\}] \quad (4)$$

where multiplication over n, denoting all the k-polarized modes, is assumed. Thus, the study of phonon spectrum via Raman scattering and IR-reflection spectroscopy is just enough for accurate determination of the lattice contribution in electro-optic effect.

The results of calculations are presented in Tables 1 and 2.

Note, that the electro-optical coefficients estimated from IR spectra for the β_i phases are larger than those measured by direct methods. The difference may be attributed to the effect of screening in strongly nonuniform layers, which reduces the 'effective' (measured) value of r_{33}, but IR-reflection and Raman scattering spectroscopy provides information about local changes of oscillators, which are responsible for the electro-optical effect.

Table 2
Frequencies ω^m (cm^{-1}) of TO and LO phonons for some A-symmetry modes of intrinsic vibrations of TaO_6 octahedron, oscillator strengths $\Delta\kappa^m$ of these modes, relative Raman scattering efficiencies $S_{zz,z}^m$ of the corresponding TO phonons normalized to scattering efficiency of TO phonon observed at 596 cm^{-1} in $LiTaO_3$ substrate, calculated ratio between electro-optic coefficient r_{33}^* in a given $H_xLi_{1-x}TaO_3$ phase and such coefficient r_{33}^o in $LiTaO_3$ substrate. The latter ratio was calculated, according to Eqs. (3) and (4), from individual lattice contributions of the A modes presented here [28]

Phase	$\varepsilon_{33} \times 10^{-3}$	ω_{TO}^m	ω_{LO}^m	$\Delta\kappa^m$	$S_{zz,z}^m$, a.u.	r_{33}^*/r_{33}^o
α	0.46	596	864	5.07	0.94	0.97
		844	827	0.02	0.05	
	0.97	596	862	5.02	0.85	0.9
		844	828	0.02	0.08	
κ	1.27	687	813	2.22	0.8	0.63
		844	860	0.076	0.08	
	2.68	687	802	2.01	0.6	0.51
		844	859	0.072	0.07	
β_1	2.82	687	795	1.88	0.5	0.48
		844	856	0.06	0.14	
		877	907	0.21	0.08	
β_2	4.09	690	772	1.38	0.35	0.37
		844	852	0.044	0.14	
		877	907	0.20	0.08	
β_3 and β_4	5.27–9.01	690	772	1.37	0.2–0.28	0.26–0.33
		844	852	0.04	0.15–0.2	
		1000	1008	0.016	0.02	

4. The nonlinear optical properties of different phases in proton exchanged lithium niobate waveguides

In the present study the reflection SHG measurements have been performed from the polished waveguide end face using the experimental set-up earlier proposed by Åhlfeldt [29] (Fig. 4). This technique circumvents the above mentioned restrictions of the reflection SHG technique with contribution from the waveguide–bulk interface and allows to measure the spatial variation in the nonlinear coefficient in the waveguides; 1.064 μm light polarized parallel to the *Z*-axis of $LiNbO_3$ from a mode-locked and Q-switched Nd:YAG laser was focused using a lens (L) (NA = 0.65) onto the polished end face of the waveguide. The waveguide sample was mounted on a piezo-electrically driven translation stage (Melles Griot X-Y-Z Nanoblock), which permitted vertical scanning both of the waveguide and the bulk region. The reflected fundamental beam and the generated reflection-SH beam were separated using beamsplitters (BS) and an interference filter (F) and detected with a germanium detector (Ge) and a photomultiplier (PM) tube, respectively. The reflected IR intensity, which was used to determine the position of the air/sample interface, was monitored using a lock-in amplifier, and the SH signal from the photomultiplier tube was analyzed with a gated integrator. The intensity of the reflected SH signal is proportional to the square of the second-order nonlinearity, therefore the measurement of harmonic power $I(2\omega)$ in both the exchanged and unexchanged regions by vertically edge scanning can be used to compare the waveguide nonlinearity with its substrate value. In our experiments, the nonlinear optical coefficients were determined by the relative measurement of intensities of reflected second harmonic for the PE region and for the unexchanged region of the same sample. The arrangement used provided a measurement of d_{33}, the largest coefficient in $LiNbO_3$ and the primary one for SHG in PE waveguides by the QPM as well as the Cherenkov matching schemes. From the response versus the depth of an untreated sample, the radius of the focused spot was estimated by the knife-edge technique [30] to be ~1 μm, which gives a reasonable spatial resolution for the characterization of the samples in this study. In each case the reflected SHG beam was also observed by sight in an eye-piece and photographed for analysis of its quality.

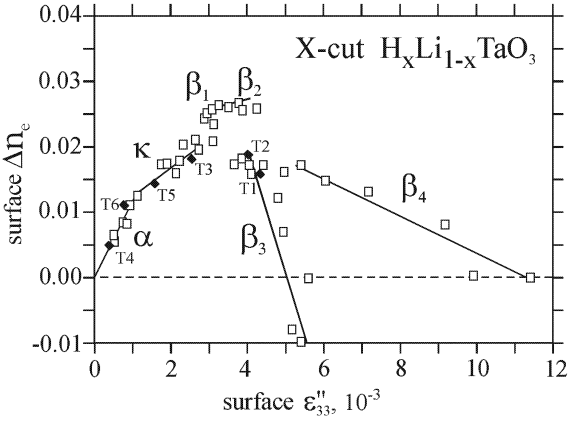

Fig. 4. Set-up for measuring nonlinear properties of PE $LiNbO_3$ or $LiTaO_3$ waveguides. L, focusing lens; F, filter; BS, beam splitter; PD1 (2ω), photodetector for second harmonic; PD2 (ω), photodetector for fundamental wavelength; $\lambda = 1.06$ μm.

It was found that for the samples, where the β_4, β_3 and β_1 phases were generated at the surface, the nonlinear coefficient in the guide is less then ~15% of the bulk value. However for the β_2 phase the d_{33} nonlinear coefficient is ~55% of the bulk value [31].

For the waveguides formed by annealing process from the β_i-phase structures and exhibited the κ_2^{LT}, κ_1^{LT} and α $H_xLi_{1-x}NbO_3$ phases at the surface, the measured intensity of the reflected SH signal that was strongly reduced after the initial proton exchange seems to be restored and even increased after annealing [31]. However, this apparent increase of nonlinearity is accompanied by a strong degradation of the quality of the SHG reflected beam in the region of initial β_i-phase PE waveguides due to the beam scattering [31]. The results obtained indicate that the possibility to make stable annealed κ_i-phase waveguides with low losses and restored nonlinearity is very doubtful. However, α-phase waveguides fabricated by soft proton exchange show nonlinear optical properties similar to bulk material.

The results obtained are summarized in Table 3.

Similar study has been performed for PE $LiTaO_3$ waveguides. The results obtained are summarized in Table 4 [32].

Table 3
Non-linear coefficient for different $H_xLi_{1-x}NbO_3$ phases [31]

Phase	d^*_{33}/d^o_{33}	Remark
β_4	<0.15	
β_3	<0.15	
β_2	0.55	
β_1	<0.15	
κ_2	–	Apparent increase of nonlinearity is accompanied by a strong degradation of the quality of the SHG reflected beam
κ_1	–	Apparent increase of nonlinearity is accompanied by a strong degradation of the quality of the SHG reflected beam
α (APE)	–	Apparent increase of nonlinearity is accompanied by a strong degradation of the quality of the SHG reflected beam
α (SPE)	~1	

5. Multifunctional integral optical chip for fiber optical gyroscope with linear digital output

The fiber optical gyros (FOG) have a significant feature, when compared with the traditional spinning mass gyros, such as short warming-up time, light weight, maintenance-free, reliability, wide dynamic range, large bandwidth and low power consumption.

One of the main fiber optical gyroscope's components is a multifunctional integrated optical chip (MIOC). Our MIOC is a solid state waveguide device on X-cut $LiNbO_3$ substrate fabricated by SPE process realized by high-temperature proton exchange method (HTPE) [21]. It includes a linear polarizer, Y-junction coupler and two pairs of electro-optic phase modulators. Light coming from the optical fiber coupler is linearly polarized within the MIOC to greater than 60 dB. This high degree of polarization minimizes bias uncertainty due to polarization non-reciprocity. The Y-junction coupler within the MIOC splits the light into equal amplitude waves, each directed along a separate waveguide within the MIOC. Each of the resulting waves pass through an electrooptical phase modulator and after two waves counterpropagate around the optical polarization maintaining (PM) optical fiber sensor coil. To achieve the low random walk and bias a 1070 m coil is used.

A very important advantage of proton exchange (PE) waveguides is the following. In such waveguides the extraordinary refraction index is increasing, while refraction index of ordinary ray is decreasing. As a result, proton exchanged waveguides support propagation only of extraordinary polarization modes (TE in our case). Therefore, it is not necessary to use a polarizer in the fiber optical gyroscope, which brings an additional loss.

It is well known that the standard technology of a PE waveguide (APE-technology) [2] applies a two-level process, which consists of a PE (melting benzoic acid as a rule) and subsequent annealing. It was recently found that different defects are formed in the surface area of the waveguide due to different phase transitions [31]. These defects are sources of additional scattering of light. HTPE, in contrast to APE, does not allow any phase transitions, and,

Table 4
Non-linear coefficient for different $H_xLi_{1-x}TaO_3$ phases [32]

Phase	d^*_{33}/d^o_{33}	Remark
β_4	<0.15	
β_3	<0.15	
β_2	0.55	
β_1	<0.15	
κ	–	Apparent increase of nonlinearity is accompanied by a strong degradation of the quality of the SHG reflected beam
α (APE)	–	Apparent increase of nonlinearity is accompanied by a strong degradation of the quality of the SHG reflected beam
α (SPE)	~1	

therefore, allows one to achieve smaller optical losses and higher electro-optical coefficients.

The modeling Y-splitter with the help of Optiwave's software 'BPC-cad' allowed us to choose an optimum function of Y-splitting.

The HTPE processes are held in the specially developed containers. Specially developed metals and dielectric films are used as masks to provide local proton exchange diffusion. Then by vacuum deposition of electrodes, the integrated electro-optical phase modulators are formed on both arms of a Y-splitter. Then the end surfaces are cut (the angle is 10 degrees to the *Y* axis), polished, and finally they are coupled with input isotropic and two output anisotropic polarization holding fibers (PANDA) with the help of an EXFO automatic aligner F-3000. The final steps are packaging and welding electrodes.

MIOC is a monoblock hermetic product, which is connected to the optical block of FOG by means of fiber waveguide welding and soldering phase modulator electrical outputs to the electronic blocks.

The main parameters of our MIOC with operating wavelength 830 ± 30 nm are the following:

optical power loss (at depolarized light), dB	<7
polarizer extinction ratio, dB	>60
division coefficient	0.5 ± 0.05
phase sensitivity of each of modulator, rad/V	>1

MIOC is a key element of our fiber optical gyro. The general block diagram of the device is shown in Fig. 5. The two waves traversing the coil recombine at the Y-junction of the MIOC. The interference results in a rotation rate-dependent intensity which propagates to the 2×2 fiber coupler (beam splitter) and then to the photodetector. A closed loop modulation scheme based on all digital serrodyne technologies is used in our FOG. It means a $\pi/2$ phase shift is imposed upon one of the counterpropagating waves relative to the other as well as the Sangac phase shift is compensated. In this case the control signal of the phase modulator can be used to measure the rotation rate. It is well known that with such an approach the output characteristic of FOG is linear and scale factor is independent from parameters of most structural components of the device. This is very important because if we process the information by means of a variable signal or a digital method, then along with the stability improvement of scale coefficient the number of the electronic factors which have an influence on the output signal error is essentially reduced.

FOG sensitivity to the rotation is mainly determined by the fiber loop design, its size, fiber type,

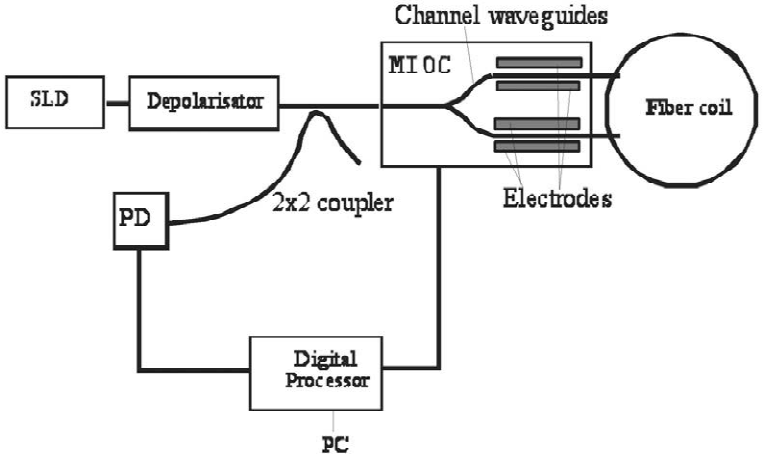

Fig. 5. Fiber-optical gyroscope minimum configuration. Digital processor is electrically connected with planar electrodes.

and the wound method. In our design we use a single-mode polarization maintaining (PM), optical fiber PANDA with strong birefringence.

FOG with the following parameters have been realized

Bias repeatability, 3σ, °/h	≤ 0.1
Random walk, °/$\sqrt{\text{h}}$	≤ 0.005
Scale factor repeatability, %	≤ 0.01

6. Conclusion

Proton exchange is a very simple and attractive technique to make optical waveguides in $LiNbO_3$ and $LiTaO_3$ crystals, but varying the fabrication parameters leads to very different waveguides with different optical, electrooptical and nonlinear properties. Knowledge of $H_xLi_{1-x}NbO_3$ and $H_xLi_{1-x}TaO_3$ single crystal phase diagrams for the popular crystal cuts enables one to predict properties of the waveguides and to optimize the fabrication process.

References

[1] W.B. Spillman, N.A. Sanford, R.A. Soref, Opt. Lett. 8 (1983) 497–499.
[2] T. Findakly, P. Suchoski, F. Leonberger, Opt. Lett. 13 (1988) 797–799.
[3] J.L. Jackel, C.E. Rice, J.J. Veselka, Appl. Phys. Lett. 41 (1982) 607–609.
[4] Yu.N. Korkishko, V.A. Fedorov, Ion Exchange in Single Crystals for Integrated Optics and Optoelectronics, Cambridge International Science, Cambridge, UK, 1999.
[5] P.G. Suchoski, T.K. Findakly, F.J. Leonberger, Opt. Lett. 13 (1988) 1050–1052.
[6] Yu.N. Korkishko, V.A. Fedorov, IEEE J. Select. Top. Quant. Electr. 2 (1996) 187–196.
[7] Yu.N. Korkishko, V.A. Fedorov, J. Appl. Phys. 82 (1997) 171–183.
[8] Yu.N. Korkishko, V.A. Fedorov, M.P. De Micheli, P. Baldi, K. El Hadi, A. Leycuras, Appl. Opt. 35 (1996) 7056–7060.
[9] V.A. Fedorov, Yu.N. Korkishko, Ferroelectrics 160 (1994) 185–194.
[10] K. El Hadi, P. Baldi, S. Nouh, M.P. De Micheli, A. Leycuras, V.A. Fedorov, Yu.N. Korkishko, Opt. Lett. 21 (1995) 223–225.
[11] D.B. Maring, R.F. Tavlykaev, R.V. Ramaswamy, Yu.N. Korkishko, V.A. Fedorov, J.M. Zavada, Appl. Phys. Lett. 73 (1998) 423–425.
[12] V.A. Ganshin, V.Sh. Ivanov, Yu.N. Korkishko, V.Z. Petrova, Sov. Phys. Tech. Phys. 31 (1986) 1313–1319.
[13] V.A. Ganshin, Yu.N. Korkishko, V.Z. Petrova, Sov. Phys. Tech. Phys 33 (1988) 686–688.
[14] V.A. Ganshin, Yu.N. Korkishko, Sov. Phys. Tech. Phys. 35 (1990) 1095–1098.
[15] J.L. Jackel, J.J. Johnson, Electron. Lett. 27 (1991) 1360–1362.
[16] Yu.N. Korkishko, V.A. Fedorov, S.V. Katin, A.V. Kondrat'ev, Proc. SPIE 2401 (1995) 149–160.
[17] V.A. Fedorov, Yu.N. Korkishko, J. Opt. Commun. 15 (1994) 155–158.
[18] K. El Hadi, M. Sundheimer, P. Aschieri, P. Baldi, M.P. De Micheli, D.B. Ostrowsky, F. Laurell, J. Opt. Soc. Am. B 14 (1997) 3197–3203.
[19] P. Baldi, M.P. De Micheli, K. El Hadi, S. Nouh, A.C. Cino, P. Aschieri, D.B. Ostrowsky, Opt. Eng. 37 (1998) 1193–1202.
[20] L. Chanvillard, P. Aschieri, P. Baldi, M. De Micheli, D.B. Ostrowsky, L. Huang, D.J. Bamford, in: Proceedings of the 9th European Conference on Integrated Optics, Torino, Italy, 1999, pp. 513–516.
[21] Y.N. Korkishko, V.A. Fedorov, O.Y. Feoktistova, IEEE J. Lightwave Technol. 18 (2000) 562–568.
[22] Yu.N. Korkishko, V.A. Fedorov, A.N. Alkaev, F. Laurell, in: Proceedings 10th European Conference on Integrated Optics, Paderborn, Germany, 2001, pp. 373–376.
[23] V.A. Fedorov, V.A. Ganshin, Yu.N. Korkishko, Physica status solidi(a) 135 (1993) 493–505.
[24] I.P. Kaminow, W.D. Johnston Jr., Phys. Rev. 160 (1967) 519–526.
[25] W.D. Johnston Jr., Phys. Rev. B 1 (1970) 3494–3501.
[26] H. Poulet, J.-P. Mathieu, Spectres de Vibration et Symetrie des Cristaux, Gordon and Breach, Paris, 1970.
[27] Yu.N. Korkishko, V.A. Fedorov, S.M. Kostritskii, J. Appl. Phys. 84 (1998) 2411–2419.
[28] S.M. Kostritskii, Yu.N. Korkishko, V.A. Fedorov, D.B. Maring, R.F. Tavlykaev, R.V. Ramaswamy, J. Appl. Phys. 91 (2002) 930–938.
[29] H. Åhlfeldt, J. Appl. Phys. 76 (1994) 3255–3260.
[30] D.K. Cohen, B. Little, F.S. Luecke, Appl. Opt. 23 (1984) 637–640.
[31] Yu.N. Korkishko, V.A. Fedorov, F. Laurell, IEEE J. Select. Top. Quant. Electr. 6 (2000) 132–142.
[32] Yu.N. Korkishko, V.A. Fedorov, A.N. Alkaev, F. Laurell, Appl. Phys. B 73 (2001) 94–97.